JOURNAL OF SOLID STATE CHEMISTRY **133,** 365–371 (1997)
ARTICLE NO. SC977583

High-Pressure, High-Temperature Syntheses in the B–C–N–O System

II. Electron Energy-Loss Spectroscopy (EELS)

Laurence A. J. Garvie,*,[1] Hervé Hubert,† William T. Petuskey,† Paul F. McMillan,† and Peter R. Buseck*,‡

*Department of Geology, †Materials Research Group in High Pressure Synthesis, and ‡Department of Chemistry and Biochemistry, Arizona State University, Tempe, Arizona 85287

Received August 4, 1997; accepted August 4, 1997

Materials with structures related to that of α-rhombohedral B (α-rh B) were synthesized in the B–C–N–O system at high pressures and temperatures. Electron energy-loss spectroscopy with a transmission electron microscope was used to determine the stoichiometry of these phases. The energy-loss near-edge structure of the core-loss edges provided qualitative information on the bonding and local band structure. Extensive solid solution between B_4C and B_6O was found in some of the syntheses as well as nanorods with composition near B_6C in one experiment. The analysis of the new α-rh B-type material, nominally B_6N, provided a mean composition of $B_6N_{0.92}$. The B K edge from B_6N is similar to that from other icosahedral boron-rich phases, more specifically to B_6O, although differences near the conduction-band onset reveal a high level of unoccupied states within the band gap. © 1997 Academic Press

1. INTRODUCTION

Elemental α-rhombohedral boron (α-rh B) is unique in forming an allotrope based on B_{12} icosahedra. The icosahedra are arranged in a slightly deformed cubic lattice with their centers at the corners of a rhombohedral unit cell. In α-rh B the intericosahedral bonds are at least as stiff as the icosahedral bonds. A unique family of compounds exist that possess the basic structure of α-rh B (1, 2, 3), with "guest" atoms either substituting for a B in the icosahedra or situated in sites along the [111] diagonal of the rhombohedral unit cell. Examples of B-rich phases with the α-rh B structure include B_4C and B_6O, the pnictides $B_{12}As_2$ and $B_{12}P_2$, and the recently described nitrides, B_6N (4) and $B_5NBe_{0.5}$ (5).

The unusual structures of borides with the α-rh B structure impart many unique properties that have important technological applications. For example, boron carbide, nominally B_4C, has a high melting point, hardness close to TiB_2, good mechanical properties, low density, high neutron absorption cross section, good chemical resistance, and is used as a grinding material and neutron absorber in nuclear reactors. While most attention has been devoted to B_4C, the properties of the numerous compounds with the α-rh B structure remain largely unstudied.

The structural similarity among compounds based on the α-rh B structure is thought to lead to solid solution. While doping has been studied for Si, P, and Al in B_4C (2, 6, 7) no true solid-solution series has been described between two end-member α-rh B-rich materials. Despite their close structural relationship, few ternary α-rh B-rich materials have been produced, e.g., $B_{10}CAl_{0.25}$, B_4CAl_x, $B_5NBe_{0.5}$, and $B_6CBe_{0.5}$.

Unless otherwise specified, the formulas B_6N and B_6O are used throughout this paper to refer to the nominally stoichiometric end members, although full occupancy of the N or O is never realized. As a result of this non-stoichiometry, formulas for the oxide and nitride end members are commonly expressed as B_6O_{1-x} and B_6N_{1-x}, respectively, where $x \leq 1$. Formulas for the icosahedral B-rich phases expressed in this manner can thus be interpreted in terms of a deficiency of the guest atom. The boron carbides with the α-rh B structure cannot be so easily expressed in this fashion because of the extended composition range that they exhibit, from ca. B_9C to the C-rich end at B_4C.

In this contribution we present parallel electron-energy loss (PEELS) results of high-pressure high-temperature syntheses of B-rich phases with the α-rh B structure containing one or more of C, N, and O. During the course of these syntheses we prepared macroscopic amounts of B_6N, a previously reported, although unsubstantiated phase. A primary goal was to study the solid solution between B_4C and B_6O end-members and to synthesize ternary phases from these end-members. Nanorods of boron carbide of

*To whom correspondence is to be addressed. E-mail: garvie@imap3.asu.edu.

0022-4596/97 $25.00

composition B_6C, with diameters of 20 nm and lengths of over 5 μm, were produced in one run.

2. EXPERIMENTAL PROCEDURES

2.1. Sample Preparation

The starting materials for the reactions were anhydrous B_2O_3 (99.99%), amorphous B (99.999%), hexagonal BN (hBN, 99.999%), and graphitic C (99.999%). Mixtures (Table 1) were pressed into pellets, placed into hBN capsules, and loaded into a Walker-type multianvil apparatus. The pressure medium consisted of an MgO octahedron, and force was applied by eight tungsten carbide cubes with corners truncated to triangular faces. Samples were pressurized to between 5 and 7.5 GPa and then heated at 1700°C for 30 min. After the reaction run, the sample was removed and selected regions were analyzed. Further details on sample preparation, scanning electron microscopy (SEM), and powder X-ray diffraction (XRD) can be found in part I of this series (4).

2.2. Electron Energy-Loss Spectroscopy

Spectra were acquired with a Gatan 666 PEELS spectrometer attached to a Philips 400ST-FEG transmission electron microscope (TEM). The TEM was operated at 100 keV, with a probe semiangle of 0.9 mrad and a collection angle of 11 mrad. Under these conditions, the resolution of the TEM PEELS system was 0.9 eV. The spectrometer was calibrated against the B K edge of hexagonal BN, which is at 192.14 eV (8).

Core-loss edges were obtained from thin areas, typically < 50 nm thick, overhanging holes in the lacy C film substrate. Spectra were acquired from areas of approximately 20 nm diameter in diffraction mode. The dark current and a background of the form AR^{-r} (9) was subtracted from beneath each core-loss edge. The edges were further processed by deconvoluting the effect of the asymmetry of the zero-loss peak and the point spread function (9). The PEELS spectra were analyzed with the Gatan el/p software and the elemental ratios determined using Hartree–Slater cross sections. Further experimental details can be found in Ref. (5).

2.3. Quantification

The height of an edge gives only an approximate guide to the amount of an element present since the near-edge region can be appreciably modified by the environment of the atom. Instead of peak heights, the integrated intensity, $I(\delta, \beta)$, within a suitable energy window, δ, is related to elemental concentration. The integrated intensity, I, depends upon the collection angle, β, since only those inelastically scattered electrons whose scattering angles lie within this angular range contribute to the core-loss edge intensity. The core-loss signal, I_x, for element x can be determined from

$$I_x(\delta, \beta) = NI\sigma_x(\delta, \beta), \quad [1]$$

where I is the incident-beam current, N the number of atoms per unit area of the specimen, and $\sigma_x(\delta, \beta)$ the cross section per atom for ionizing an inner-shell electron from atom x. Elemental quantification may be achieved by either determining the total number of atoms per unit area or via the atomic ratio method. Since determination of the total number of atoms in a unit area is difficult and not required for determination of stoichiometries, the ratio method was used. The atomic ratio between two elements x and y may be determined from

$$\frac{N_x}{N_y} = \frac{I_x(\delta, \beta)\sigma_y(\delta, \beta)}{I_y(\delta, \beta)\sigma_x(\delta, \beta)}. \quad [2]$$

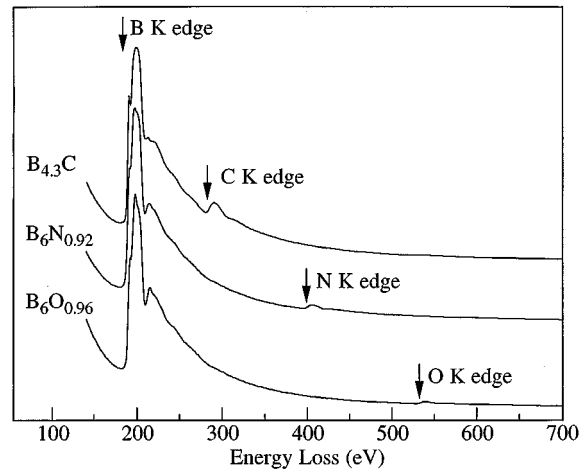

FIG. 1. Low-resolution PEELS spectra of $B_{4.3}C$, $B_6N_{0.92}$, and $B_6O_{0.96}$ showing the intense B K edge at 190 eV and weak C, N, and O K-edge onsets at 285, 400, and 530 eV, respectively.

The PEELS spectra, acquired at an energy dispersion of 1 eV, span a sufficiently wide energy range to include the B, C, N, and O K edges in the same spectrum, thus facilitating quantification. The low-resolution spectra are all similar, with an intense B K edge and the weaker K edges of the host atoms situated on the sloping background (Figs. 1 and 2). At least two spectra were acquired from each acquisition point; each spectrum was analyzed separately and their results averaged. The difference between the two sets of data from each analysis region was consistently less than $\pm 10\%$. The accuracy of the quantification for the light elements is generally better than $\pm 10\%$ as shown for the following standards analyzed by PEELS: hBN–$BN_{0.98(\pm 0.06)}$,

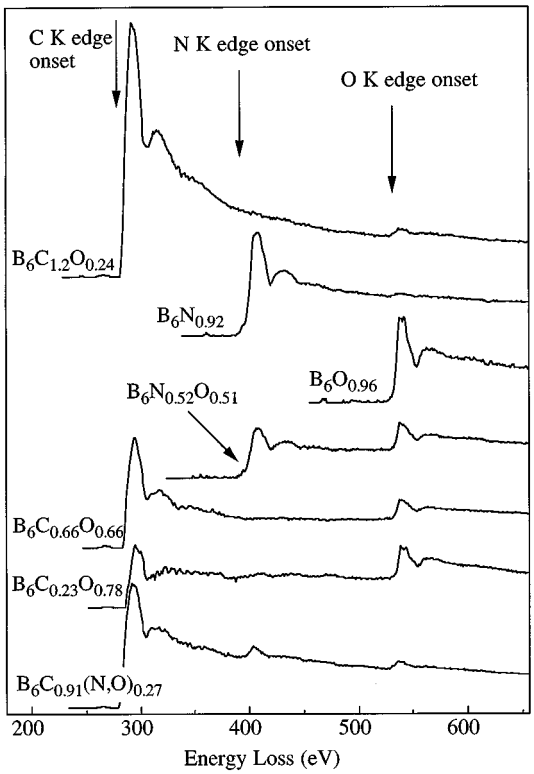

FIG. 2. Low-resolution PEELS spectra of selected run products after subtraction of the background before the first element detected following the B K edge. The background-subtracted spectra show the relationship between the peak heights of the C, N, and O K edges.

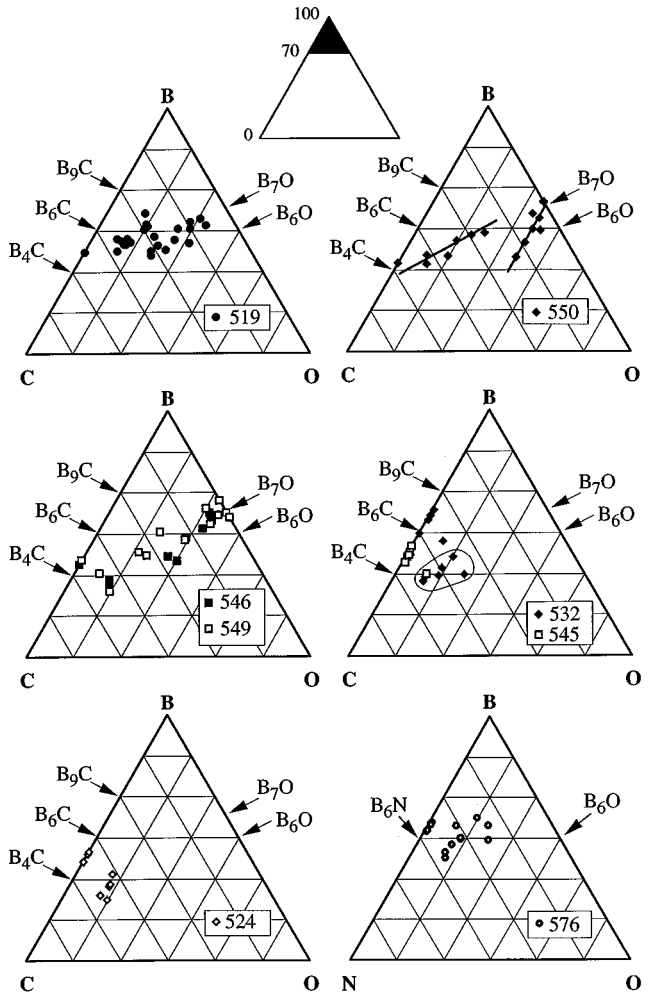

FIG. 3. Ternary B–C–O plots and B–N–O plot of α-rh B-rich materials synthesized at high pressures and temperatures. Sample numbers are indicated in the boxes, and each point represents a single analysis. For sample 532, the circled region groups the analyses from the nonfibrous materials. The lines in 550 illustrate the two different sets of materials as described in the text. The small plot at the top of the figure represents the field for the ternary plots. In these plots compositional lines are drawn at every 5 at.%.

cubic BN–$BN_{1.00(\pm 0.02)}$, CrB_2–$CrB_{2.1(\pm 0.1)}$, and BeB_2–$BeB_{2.0(\pm 0.2)}$. The accuracy of the analysis was limited by systematic errors in the theoretical cross sections and the power-law fit for the background, rather than by counting statistics. Counting statistics become a limiting factor for quantitative analysis for low elemental concentrations because the weak core-loss edge must be extracted from the backgrounds. The detection limits for C, N, and O were estimated to be between 0.1 and 1 at.%. For example, while the O K edge from roughly 1 at.% O is still visible, its edge is so weak that quantification using the standard AE^{-r} background subtraction routine and calculating a cross section over an extended energy range of the background-subtracted spectrum is difficult. Quantification of low concentrations of C was difficult because its K edge rests on the extended fine-structure oscillations of the B K edge, which make it difficult to use the standard AE^{-r} background subtraction routine.

3. ALPHA-RHOMBOHEDRAL BORON-RICH MATERIALS

3.1. Stoichiometry

The runs can be divided into those in which products are primarily close to an end-member composition and those in which intermediate compositions formed (Fig. 3). The end-member B–O and B–N phases are never fully stoichiometric, and syntheses designed to produce stoichiometric B_6O and B_6N gave $B_6O_{0.96(\pm 0.08)}$ (11) and $B_6N_{0.92(\pm 0.05)}$, as discussed below. No runs were done with only B and C. Experiments with B, C, and B_2O_3 resulted in the formation of ternary and quaternary phases. The quaternary phases formed when N from the hBN capsule was partially exchanged for the O from the B_2O_3 in the starting material. To compare the changes in stoichiometry for the ternary and quaternary α-rh B-rich materials, the formulas are expressed as $B_6C_xN_yO_z$.

TABLE 1
Summary of Syntheses

Run	Initial mixture	P(GPa)	T (°C)	t (min)
519	$16B + 2C + 3B_2O_3$	7.5	1700	30
521	$16B + 4C + 3B_2O_3$	7.5	1700	30
524	$16B + 4C + 3B_2O_3$	5	1700	5
532	$16B + 4C + 3B_2O_3$	7.5	1700	30
545	$16B + 4C + B_2O_3$	7.5	1700	30
546	$16B + 2C + B_2O_3$	7.5	1700	30
549	$16B + 2C + B_2O_3$	7.5	1700	300
550	$16B + C + B_2O_3$	7.5	1700	30
576	$5B + BN$	7.5	1700	30
451	$16B + 2B_2O_3$	5.5	1800	5
555	$16B + B_2O_3$	7.5	1700	30

The run products are polycrystalline, with variable amounts of soluble boron oxide. Spectra were acquired from separate grains after crushing and washing a small portion of the boule in water. X-ray diffraction of the insoluble material shows predominantly phases with the α-rh B structure, although small but variable amounts of cubic BN, hBN, and amorphous material are present (4). The amount of N detected in the grains depended on the proximity of the analyzed grains to the edge of the boule. In general, the largest N concentration was detected from grains close to the hBN capsule, and little to no N was detected in samples from the boule center. Only one run, 524, produced single crystals that could be separated from the soluble boron oxide by washing in water.

Phases near B_4C. Three runs, 524, 532, and 545, produced grains with compositions near B_4C; they have small but variable amounts of O. The products of samples 532 and 524 have the largest spread of data, with up to 7 at.% O from one grain from 532, corresponding to an ideal formula of $B_6C_{1.1}O_{0.33}$. In the ternary plots (Fig. 3) the apparent lower O limit corresponds to roughly 3 at. %, but this limit is an artifact of the quantification method used as discussed in Section 2.3.

Runs 532 and 524 have the same starting compositions and were run at the same temperature but at different pressures and durations (Table 1). The products in both cases can be represented as $B_6C_xO_y$, with x from 0.82 to 1.3 and y up to 0.45. The experiment with the longer heating time produced a wider range of stoichiometries and more incorporated O. In run 532 both fibers and grains were synthesized. The fibers have a maximum O content of 2.9 at.% and a minimum C content of 12.1 at.%, while the flakes exhibit an extended composition range that parallels that seen in runs with starting B to C ratios greater than 4 (see below). Run 524 differed from 532 and 545 by containing a homogenous product consisting of euhedral crystals with composition $B_{6.0(\pm 0.12)}C_{1.28}O_{0.31(\pm 0.04)}$. They are up to 20 μm in diameter and occur in a soluble boron oxide matrix.

Phases from B_4C to B_6O. Runs 519, 546, 549, and 550 produced materials that can be divided into three types depending on the starting C to B_2O_3 ratios (Table 1).

In run 519, the $C : B_2O_3$ is 2 : 3 and the grains have a range of compositions although there is a paucity of end-member compositions, i.e., no B_6O or B_4C. A line can be fitted through the data that passes through the B–C composition range near B_5C and between B_6O and B_7O on the B–O line.

TABLE 2
Physical Properties of Selected Run Products with the α-rh B Structure

Run	Physical and visual properties	TEM and EELS
519	Friable reddish brown powder.	Compositions range from $B_{6.5}C$ with minor N and O to $B_6C_{0.66}O_{0.66}$ and $B_6C_{0.45}O_{0.77}$.
524	Friable white matrix with embedded crystals. Crystals are copper coloured in reflected light and dark reddish brown in transmitted light.	Crushed crystals with average composition $B_{6.0(\pm 0.12)}C_{1.28}O_{0.31(\pm 0.04)}$.
532	Hard brownish red crystals in friable matrix.	(a) Large anhedral particles of boron carbide typically $B_6C_{1.1}O_{0.33}$. (b) Small euhedral to anhedral grains of boron carbide with minor O. (c) Boron carbide rods with typical composition $B_{6.8}C$ with minor O.
550	Black well-sintered lump with transparent red areas.	Interlocking euhedral to anhedral grains. Dominantly B_6O and B_4C although intermediate compositions also present. Typical compositions are $B_6C_{0.2}O_{0.83}$, $B_6C_{0.63}O_{49}$, to $B_6C_{1.2}O_{0.24}$.
549	Well-sintered black lump with transparent red areas.	(a) Anhedral grains with compositions $B_6C_{1.28}O_{0.2}$ to $B_6C_{0.58}O_{0.46}$. (b) Nanometer-sized euhedral to subhedral particles with average composition $B_6O_{0.85}$.
576	Well-sintered black mass, with metallic lustre.	Interlocking euhedral to subhedral grains of B_6N with minor B_4C, cubic BN, and B. Average composition of the O-free B_6N is $B_6N_{0.92}$. A range of compositions up to $B_6N_{0.48}O_{0.56}$ occur.

The product for run 550 is hard, mainly black, with transparent red areas. The $C:B_2O_3$ is 1:1, and some of the analyzed grains have compositions close to B_7O with a few at.% C. There are two compositional trends. A boron oxide close to B_7O corresponds to the red transparent areas. These compositions follow a line that parallels the 10 and 15 O at.% lines, with an average O of 12.1 ($\pm$ 0.9) at.%. These materials range from $B_6C_{0.45}O_{0.9}$ to $B_6O_{0.8}$. The second trend extends from $B_{4.2}C$ to $B_6C_{0.58}O_{0.52}$ and is for the black grains.

The starting $C:B_2O_3$ ratio was 2:1 in runs 549 and 546. Run 549 was held at 1700°C for 5 h and 546 for 30 min. The run products are similar to 550: hard and sintered with opaque black and transparent red areas. The spread of compositions is similar for both runs. Holding the high temperature for an order of magnitude more in time had little effect on the final compositions. The results show a clustering of compositions around B_7O and B_4C, with a number of analyses spanning the intervening compositions.

Phases close to B_6N. Run 576 consists of interlocking anhedral grains forming a hard, sintered, mass. The O-free grains have a mean composition of $B_6N_{0.92(\pm 0.05)}$. Up to 7 at.% O was found in some grains, these correspond to $B_6N_{0.5}O_{0.5}$ (Fig. 3). The O presumably came from O in the amorphous B used in the synthesis as up to 1 at.% O was detected by PEELS in most particles. Note, the O in the amorphous B is caused by the formation of a thin boron oxide on the particles when exposed to the air.

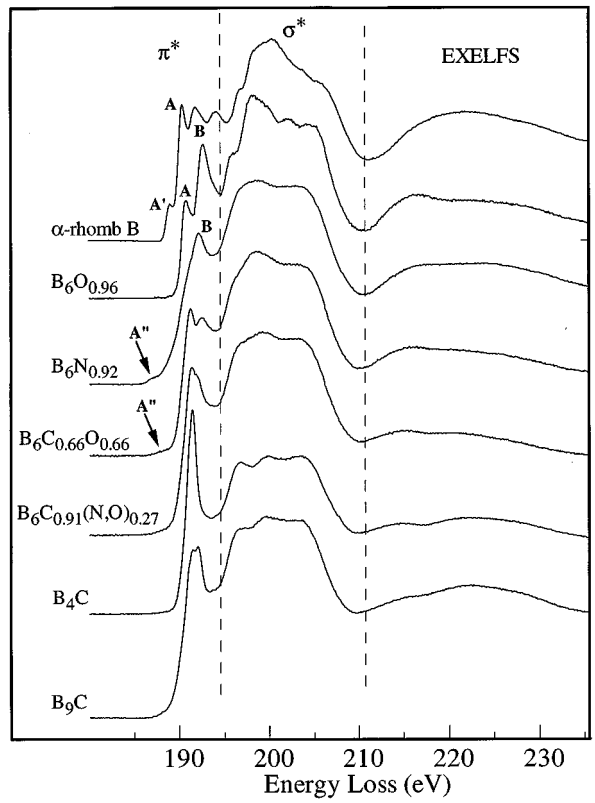

FIG. 4. Boron K edges from several α-rh B-bearing materials. The B K edges is divided into the energy-loss near-edge structure (ELNES) and extended electron-loss fine structure (EXELFS). The ELNES for the B K edges from α-rh B and the structurally related materials can be divided into the π* and σ* regions. The letters refer to features described in the text.

3.2. Energy-Loss Near-Edge Structure

The B K-edge energy-loss near-edge structure (ELNES) of α-rh B and the products with the α-rh B-structure exhibit an edge rich in features (Fig. 4). The B K-edge shapes from the α-rh B-bearing materials can be divided into three types: α-rh B, B_6O, and B_4C. Materials with intermediate compositions have B K ELNES that are a combination of the end-member edge shapes. For example, the B K edge from $B_6C_{0.66}O_{0.66}$ can be reproduced by a combination of the B K edges from B_6O and B_4C.

The B K edges arise from transitions of the *B* 1*s* electron to unoccupied states of *p*-like symmetry. In the absence of band-structure calculations that show the atom-resolved partial density of unoccupied states, the ELNES of the core-loss edges must be interpreted qualitatively. Many calculations of the α-rh B-type compounds exist for the occupied or valence band states (e.g., 11–16), although few show more than the first few eV of the conduction band. The first 20 eV of the ELNES represents the symmetry-dependent unoccupied density of states (DOS); in this case the *p*-like states hybridized with the appropriate host atom states. This DOS region is separated by a trough at ca. 210 eV from the extended energy-loss fine structure (EXELFS).

The band gap of the α-rh B-bearing materials varies from ca. 1 eV in B_4C, which is a semiconductor, to 2 and 3 eV in α-rh B and $B_{12}As_2$, respectively. Optical measurements show a band of high density of unoccupied states ca. 0.2 eV above the valence band in many α-rh B-rich materials, whereas in β-rh B up to five trapping levels have been detected within the band gap (17). Since the α-rh B structure is electron deficient from the point of view of forming a covalently bonded network with two-center bonding, interstitial atoms are required to saturate the covalently bonded network. Addition of these interstitial atoms, either between or within the icosahedra, produces large changes in the electronic, optical, and vibrational properties of these solids.

Looking first at α-rh B (Fig. 4), the first 5 eV of the B K edge contains four peaks. The sharp features represent transitions to discreet unoccupied bands formed from the intraicosahedral B–B bonds of 1.73 to 1.79 Å; strong, short, two-center intericosahedral B–B bonds (1.67 Å) along the *c*-axis; and the weak B–B (2.03 Å) bonds associated with

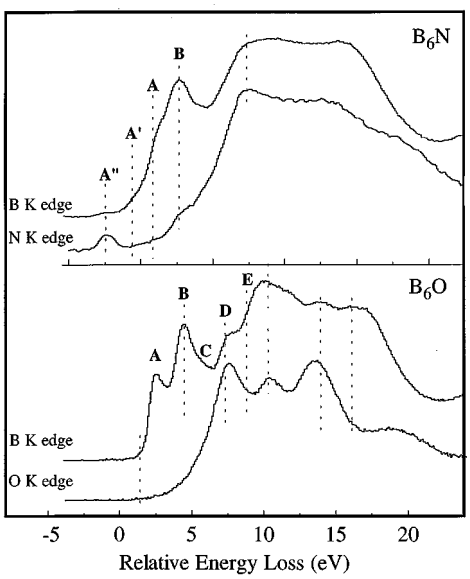

FIG. 5. Comparison between the B and N K edges of B_6N, and the B and O K edges from B_6O aligned on a relative energy scale. The estimated onset of the conduction band is marked at 0 eV.

intericosahedral three-center bonding in the $(001)_{rh}$ plane. By analogy with other B K edges (18), the peaks within the first ca. 5 eV of the B K edge represent transitions to unoccupied π^*-like states and the broad 15 eV region to σ^* states. Addition of atoms within the icosahedra, as in B_4C, has a large effect on the π^* region whereas addition of atoms between the icosahedra, as in B_6O, results in more minor near-edge changes.

Addition of O to α-rh B to form B_6O results in a shorter two-center intericosahedral bond and longer intraicosahedral bonds than in α-rh B (19, 20). The B K edge of B_6O is similar to that of α-rh B, except for the loss of the pre-edge feature, A′, and enhancement in intensity of peak B compared to the B K edge from α-rh B. The similar σ^* edge shapes between α-rh B and B_6O implies that the energy bands higher in the conduction band are largely unaffected by the O between the icosahedra. Through comparison of the B and O K edges (Fig. 5) from B_6O we deduce that the lower part of the conduction band is dominated by unoccupied B *p*-like states with only minor contribution for O *p*-like states. The slow rise in intensity of the O K edge over an 8-eV energy range does not occur for the O K edge from other materials. This slow rise in intensity indicates a broad band of O *p*-like states over the whole of the lower part of the conduction band.

In (4) we argue for a structural similarity between B_6N and B_6O, i.e., N_2 pairs between the icosahedra along the $[111]_{rh}$ diagonal. The B K edge of B_6N is similar to that of B_6O, although there are considerable differences in the σ^* region where it more closely resembles that of B_4C. In the π^* region of B_6N there are three weak features below peak B (Fig. 5). Peak A″ is lower in energy than any ionization features from the B K edge of α-rh B. A similar prepeak also occurs at the B K edges of $B_6C_{0.66}O_{0.66}$ and $B_6CBe_{0.5}$ (5). A common feature of these three materials with the prepeak is that they are gray or black with a metallic luster. It is possible that the prepeak arises from transitions of the core electrons to high densities of unoccupied states within the band gap. Such band-gap states, or trapping levels, have been detected by optical measurements in β-rh B (17) and found to be important for the electronic-transport properties.

4. CONCLUSIONS

In this investigation materials with the α-rh B structure were synthesized in the B–C–N–O system. EELS with a TEM is ideal for characterizing these materials since the K edges are well separated in energy, allowing easy determination of the elemental ratios. In addition, the ELNES of the core-loss edges provides qualitative information on the bonding and local band structures.

We show the first evidence of extensive solid solution between B_4C and B_6O. Boron carbide crystals containing a significant amount of O, for example $B_6C_{1.1}O_{0.33}$ and $B_6C_{1.28}O_{0.31}$, were obtained for mixtures in which B and C were reacted with excess B_2O_3. Nanorods with composition near B_6C were grown in one experiment.

Analyses of the new α-rh B-rich boron nitride, nominally B_6N, provide a mean composition of $B_6N_{0.92}$. The B K edge from B_6N is similar to that of B_6O although differences near the conduction band onset reveal a high level of unoccupied states within the band gap for B_6N, a sign that it may possess useful thermal and electrical properties. It is possible that these interband states impart significant metallic conductivity to B_6N. The initial experiments on B_6N suggest considerable solid solution between it and B_4C and B_6O.

ACKNOWLEDGMENTS

We thank T. Aselage (Sandia National Labs) for supplying samples of α-B, $B_{4.3}C$, and B_9C and P. Rez (Arizona State University) for his stimulating discussions on near-edge structure. This study was supported by the grants from the National Science Foundation, EAR-9219376 (to L.A.J.G. and P.R.B.) and MRG DMR-91-21570. EELS spectra were acquired at the Center for High Resolution Electron Microscopy, which is also supported by the National Science Foundation, Grant DMR-8611609.

REFERENCES

1. T. L. Aselage, D. R. Tallant, J. H. Gieske, S. B. van Deusen, and R. G. Tissot, *in* "The Physics and Chemistry of Carbides, Nitrides and Borides," NATO ASI Series E, Vol. 185, pp. 97–111. 1989.
2. T. Lundström, *in* "Boron-Rich Solids, AIP Conference and Proceedings" (D. Emin, T. Aselage, C. L. Beckel, I. A. Howard, and C. Wood, Eds.), Vol. 231, pp. 186–192. Am. Inst. of Phys., New York, 1991.
3. T. Lundstrom and H. Bolmgren, *Jpn. J. Appl. Phys.* **10,** 1 (1993).

4. H. Hubert, L. A. J. Garvie, P. R. Buseck, W. T. Petuskey, and P. F. McMillan, *J. Solid State Chem.* 356 (1997).
5. L. A. J. Garvie, P. R. Buseck, and P. Rez, *J. Solid State Chem.* **133,** 347 (1997).
6. H. Werheit, U. Kuhlmann, M. Laux, and R. Telle, *Jpn. J. Appl. Phys.* **10,** 86 (1993).
7. T. L. Aselage, D. R. Tallant, D. Elmin, S. B. van Deusen, and P. Yang, *Jpn. J. Appl. Phys.* **10,** 58 (1993).
8. L. A. J. Garvie, A. J. Craven, and R. Brydson, *Am. Mineral.* **80,** 1132 (1995).
9. R. F. Egerton "Electron Energy-Loss Spectroscopy in the Electron Microscope," Plenum, New York, 1986.
10. H. Hubert, L. A. J. Garvie, B. Devouard, P. R. Buseck, W. T. Petuskey, and P. F. McMillan, *J. Solid State Chem.* (1997).
11. A. C. Switendick, *in* "Materials Research Society Symposia Proceeding," (O. Emin, T. L. Aselage, and C. Wood, Eds.), Vol. 97, pp. 45–50. Materials Research Society, 1987.
12. A. C. Switendick, *in* "The Physics and Chemistry of Carbides, Nitrides and Borides," NATO ASI Series E, Vol. 185, pp. 525–553. 1989.
13. D. W. Bullett, *in* "The Physics and Chemistry of Carbides, Nitrides and Borides," NATO ASI Series E, Vol. 185, pp. 513–523. 1989.
14. D. W. Bullett, *in* "Boron-Rich Solids, AIP Conference and Proceedings" (O. Emin, T. L. Aselage, C. L. Beckel, I. A. Howard, and C. Wood, Eds.), Vol. 231, pp. 21–28. Am. Inst. of Phys., New York, 1991.
15. D. W. Bullett, *Jpn. J. Appl. Phys.* **10,** 31 (1993).
16. L. Kleinman, *in* "Boron-Rich Solids, AIP Conference and Proceedings" (O. Emin, T. L. Aselage, C. L. Beckel, I. A. Howard, and C. Wood, Eds.), Vol. 231, pp. 13–20. Am. Inst. of Phys., New York, 1991.
17. H. Werheit, *Jpn. J. Appl. Phys.* **10,** 66 (1993).
18. L. A. J. Garvie, D. Emin, P. Rez, and P. R. Buseck, to be submitted for publication.
19. M. Kobayashi, I. Higashi, C. Brodhag, and F. Thevenot, *J. Mater. Sci.* **28,** 2129 (1993).
20. H. Bolgren, T. Lundstrom, and S. Okada, *in* "Boron-Rich Solids, AIP Conference and Proceedings" (O. Emin, T. L. Aselage, C. L. Beckel, I. A. Howard, and C. Wood, Eds.), Vol. 231, pp. 197–200. Am. Inst. of Phys., New York, 1991.